European Polymer Journal 46 (2010) 910–917

Contents lists available at ScienceDirect

European Polymer Journal

journal homepage: www.elsevier.com/locate/europolj

Macromolecular Nanotechnology

Effect of the silica content on the physico-chemical and relaxation properties of hybrid polymer/silica nanocomposites of P(EMA-*co*-HEA)

A. Vallés-Lluch [a,b,*], G. Gallego Ferrer [a,b,c], M. Monleón Pradas [a,b,c]

[a] Center for Biomaterials and Tissue Engineering, Universidad Politécnica de Valencia, Cno. de Vera s/n, 46022 Valencia, Spain
[b] Regenerative Medicine Unit, Centro de Investigación Príncipe Felipe, Av. Autopista del Saler 16, 46013 Valencia, Spain
[c] Networking Research Center on Bioengineering, Biomaterials and Nanomedicine, Valencia, Spain

ARTICLE INFO

Article history:
Received 4 November 2009
Received in revised form 27 January 2010
Accepted 6 February 2010
Available online 13 February 2010

Keywords:
Nanocomposite
Acrylate
Silica
Sol–gel
Bioactivity

ABSTRACT

Poly(ethyl methacrylate-*co*-hydroxyethyl acrylate) 70/30 %wt/silica, P(EMA-*co*-HEA)/SiO_2, nanocomposites, with silica contents ranging from 0 to 30 %wt, were synthesized and studied as promising candidate materials for the synthetic matrix of scaffolds for bone substitutes or dentin regeneration. The physico-chemical properties of the hybrids were studied by calorimetry and by contact angle measurements on the surfaces. The dynamic-mechanical and compression properties were analysed. Intermediate silica contents in the range from 10 to 20 %wt of silica rendered co-continuous interpenetrated structures, in which silica produced a reinforcing effect in the polymeric matrix and at the same time conferred bioactivity to the surfaces by improving surface wettability, making these hybrids appropriate for the proposed application. On the contrary, silica percentages below 10 %wt formed disconnected inorganic aggregates at the nanoscale dispersed in the copolymer matrix, which did not modify significantly the copolymer properties. Silica contents above 20 %wt formed denser inorganic networks with few terminal silanol groups available at the surfaces, much more rigid and hardly manageable samples.

1. Introduction

Biomaterials for guided mineralized tissue regeneration need to be biocompatible, osteoinductive or osteoconductive, and mechanically compatible with native bone. Since the discovery of Bioglass® (45% SiO_2, 24.5% CaO, 24.5% Na_2O, 6% P_2O_5) by Hench et al. in 1971 [1], which appeared to strongly adhere to bone tissue, glasses with different compositions and glass ceramics have been developed, and their ability to precipitate bone-like apatite on their surface has been investigated [2–12]. In 1991 Kokubo demonstrated that materials able to precipitate apatite on their surfaces in the living body, all induced the nucleation of bone-like apatite on their surface when soaked in an acellular simulated body fluid (SBF) (with ion concentrations very similar to those of the human blood plasma) [3,13]. This *in vitro* test in SBF has been since then commonly employed to predict the so-called bioactivity of materials before animal testing.

Silica plays a fundamental role in bioactive glasses [12,14] because in physiological ambient (pH 7.4), silica is negatively charged and silanol groups are formed on the surface by ion interchange of alkali ions with protons of the medium. The negative charge of the surface silanol groups interacts with positive calcium ions, forming calcium compounds such as amorphous calcium silicate. These calcium compounds possess positive charge and consequently combine with the phosphate negative ions from the fluid, forming an amorphous calcium phosphate that finally crystallizes to give hydroxyapatite similar to bone. These valuable features have allowed bioactive glasses to be used in bone grafts, maxillofacial, ear, nose or throat applications [12]. Glasses can be cast to plates,

* Corresponding author. Address: Center for Biomaterials and Tissue Engineering, Universidad Politécnica de Valencia, Cno. de Vera s/n, 46022 Valencia, Spain. Tel.: +34 963877277; fax: +34 963877276.
E-mail address: avalles@ter.upv.es (A. Vallés-Lluch).

0014-3057/$ - see front matter © 2010 Elsevier Ltd. All rights reserved.
doi:10.1016/j.eurpolymj.2010.02.004

rods, etc. or be used as filler materials in the form of particulates, but their brittleness makes difficult their use in load-bearing applications.

The incorporation of polymeric components to sol–gel silica derived materials constitutes an interesting alternative to improve the mechanical properties and design different structures, or to provide more compatible media for encapsulation of biological molecules and medicines. In sol–gel silica hybrids, the silica network is expected to reinforce mechanically the organic matrix and at the same time confer bioactivity to the hybrids.

Bearing in mind that materials suited for dental applications should be mechanically resistant and, at the same time, have good interfacial contact with biological fluids, a combination of two comonomers was chosen for the present study. A 70/30 %wt hydrophobic/hydrophilic copolymer of poly(ethyl methacrylate-*co*-hydroxyethyl acrylate), P(EMA-*co*-HEA), has been employed herein to obtain silica-based hybrids, as promising candidate materials for the synthetic matrix of scaffolds for bone or dentin regeneration. This copolymer has been chosen because of its balanced properties: good mechanical properties provided by EMA and hydrophilicity of HEA needed for the efficient penetration of biological fluids into porous structures and for good miscibility with the inorganic mixture. The synthesis procedure is described in detail in a previous work, and the structure of silica in the polymeric matrix of the obtained nanohybrids has been analysed [15]. This work aims at characterizing these hybrids by means of contact angle measurements, differential scanning calorimetry, dynamic-mechanical analyses and compression mechanical tests, and to relate their properties with their respective different morphologies.

2. Materials and methods

2.1. Materials

The hybrids were obtained by the copolymerization of ethyl methacrylate, EMA (99%, Aldrich) and hydroxyethyl acrylate, HEA (96%, Aldrich), with a 70/30 %wt monomers ratio, during the simultaneous acid-catalyzed sol–gel polymerization of tetraethoxysilane, TEOS (98%, Aldrich), following the procedure described in a previous work [15]. Briefly, an organic solution was obtained by mixing the organic monomers with a 0.5 %wt of ethylene glycol dimethacrylate, EGDMA (98%, Aldrich), as crosslinking agent and a 2 %wt of benzoyl peroxide, BPO (97%, Fluka), as thermal initiator, while a TEOS solution was prepared by mixing with distilled water and hydrochloric acid (37%, Aldrich) in the molar ratio 1:2:0.0185, respectively. After 30 min of stirring, both solutions were mixed and stirred for another 30 min.

The monomeric mixture was polymerized in an oven at 60 °C for 21 h and post-polymerized at 90 °C for 18 h to obtain sheets of 0.8 mm thickness, which were afterwards rinsed in a boiling distilled water/ethanol mixture for 24 h to eliminate monomer residues, eventually allowed to dry in a vacuum desiccator at 80 °C until constant weight, and kept in those conditions until measurements. All measurements were thus made on samples which could be regarded as dry; this was furthermore supported by the absence of any trace of humidity in the TGA thermograms. Thus, sheets of poly(ethyl methacrylate-*co*-hydroxyethyl acrylate), P(EMA-*co*-HEA) 70/30 %wt, with varying proportions of silica, SiO_2, up to 30 %wt could be obtained. Hereafter these hybrids will be referred to as Hx, x being the percentage of silica in the sample. Sheets of the homopolymers poly(ethyl methacrylate), PEMA, and poly(hydroxyethyl acrylate), PHEA, were obtained following the same procedure as reference materials.

2.2. Methods

Thermogravimetric analyses, TGA, were done in a TA-SDT Q600 thermobalance (TA Instruments, New Castle, DE, USA) with approximately 7 mg of sample accurately weighed in standard alumina crucibles. The temperature was raised from 25 to 1000 °C at a rate of 10°C min^{-1} under a nitrogen flow of 50 ml min^{-1}. The TGA thermograms and the decomposition residues were used to assess that the silica precursor was efficiently hydrolysed and condensed to silica during the sol–gel process.

The surface energies of the bulk samples were determined by measuring the contact angle on the surface of the samples of drops of three different liquids: water (extra pure, Scharlau), formamide (99.5%, Aldrich) and diethylenglycol (99%, Aldrich). A Dataphysics OCA instrument (DataPhysics Instruments GmbH, Filderstadt, Germany) was used for this purpose. A minimum of 10 drops of each liquid were analysed for each composition.

The Young equation [16] has been considered:

$$\gamma_{sl} = \gamma_s - \gamma_l \cdot \cos\theta \tag{1}$$

where γ_{sl}, γ_s, and γ_l are the solid–liquid, solid–vapor and liquid–vapor interfacial tensions, respectively, and θ is the contact angle of the liquid on the surface. This equation has been combined with the relation by Owens and Wendt [17], which makes the following ansatz for the interfacial tension γ_{sl} in terms of the dispersive, γ^d, and polar, γ^p, contributions to γ:

$$\gamma_{sl} = \gamma_l + \gamma_s - 2 \cdot (\gamma_l^d \cdot \gamma_s^d)^{1/2} - 2 \cdot (\gamma_l^p \cdot \gamma_s^p)^{1/2} \tag{2}$$

From Eqs. (1) and (2), the following equation can be obtained:

$$\frac{1+\cos\theta}{2} \cdot \frac{\gamma_l}{(\gamma_l^d)^{1/2}} = (\gamma_s^d)^{1/2} + \left(\frac{\gamma_l^p}{\gamma_l^d}\right)^{1/2} \cdot (\gamma_s^p)^{1/2} \tag{3}$$

γ_l and its components are tabulated for the different liquids (water, formamide and diethylenglycol) in Table 1 and θ are the measured contact angles of drops of these liquids

Table 1
Liquids employed in the contact angle measurements, surface tensions (γ_l), and their dispersive (γ_l^d) and polar (γ_l^p) components [18,19].

Liquid	γ_l (mN/m)	γ_l^d (mN/m)	γ_l^d (mN/m)
Water	72.10	19.90	52.20
Diethylenglycol	45.21	35.91	9.30
Formamide	56.90	23.50	33.40

on the surfaces of the dry samples. Representing $\frac{1+\cos\theta}{2}\cdot\frac{\gamma_l}{(\gamma_l^d)^{1/2}}$ *vs.* $\left(\frac{\gamma_l^p}{\gamma_l^d}\right)^{1/2}$, the surface tensions of the samples surfaces, γ_s, and their dispersive, γ_s^d, and polar, γ_s^p, components, can be obtained from the *y*-ordinate and the slope, respectively, of a least-square linear fit of experimental data to Eq. (3).

Differential Scanning Calorimetry, DSC, measurements were performed in a Mettler Toledo DSC 823e (Mettler-Toledo Inc., Columbus, OH, USA) to determine the thermal properties of the samples. Each test specimen consisted of approximately 8 mg of material accurately weighed in a standard aluminium pan and sealed. The pans were scanned from room temperature to 150 °C at a heating rate of 10 °C min^{-1} to eliminate the thermal history of the materials, cooled to −50 °C at 40 °C min^{-1} and reheated to 200°C at 10°C min^{-1}, under nitrogen atmosphere. Calibration was made with indium and zinc standards.

Dynamic-Mechanical Spectroscopy, DMS, was performed in the tension mode at 2°C min^{-1} in a Seiko DMS210 instrument (Seiko Instruments Inc., Chiba, Japan), from −60 to 200°C at a frequency of 1 Hz. Specimens were rectangular shaped, approximately 25 × 6.5 × 0.8 mm^3.

Mechanical compression tests were performed in a Seiko TMA/SS6000 device (Seiko Instruments Inc., Chiba, Japan), from 0.05 to 150 g at 10 g min^{-1}, at room temperature. Specimens were disk shaped and each composition set consisted of five replicas. The compressive elastic moduli, *E*, were obtained from the initial slope of the stress–strain curves, after disregarding the initial convex zone due to lack of parallelism of the surfaces, in order to ensure that the load was homogeneously distributed on the surfaces.

3. Results

Table 2 presents the average water contact angles, θ_w, and the surface tensions, γ_s, with the dispersive, γ_s^d, and polar, γ_s^p, components, calculated as explained from the contact angle measurements with the three liquids: water, formamide and diethylenglycol. The polarity of the surfaces has been calculated for the different samples as the polar contribution divided by the surface tension, γ_s^p/γ_s, and is also displayed in Table 2.

The water contact angle of the H05 surface is identical to that of the copolymer, decreases for the intermediate silica contents and increases again for the H30 surface, taking again a similar value to that of the copolymer.

Table 2
Water contact angle (θ_w), surface tensions (γ_s) with polar (γ^p) and dispersive (γ^d) components, and polarity (γ^p/γ_s).

Sample	θ_w (°)	γ_s (mN/m)	γ^p (mN/m)	γ^d (mN/m)	γ^p/γ_s
PEMA	82.6 ± 1.6	33.4	6.7	26.7	0.20
PHEA	96.1 ± 3.9	24.7	9.8	14.9	0.39
H00	91.8 ± 2.3	26.1	3.9	22.2	0.15
H05	92.0 ± 1.6	23.2	4.9	18.3	0.21
H10	80.1 ± 2.9	31.9	9.1	22.8	0.28
H15	76.5 ± 1.4	34.0	9.9	24.2	0.29
H20	76.8 ± 4.1	31.2	11.6	19.6	0.37
H30	90.5 ± 2.2	24.5	5.2	19.3	0.10

The surface tension of PHEA is lower than that of PEMA, due to a decrease in the dispersive component, the polar component being slightly higher. The surface tension of the copolymer takes an intermediate value between those of the homopolymers, with a dispersive component between those of them, but with the polar component lower. Concerning the hybrids, the surface tension slightly decreases when adding a 5 %wt of silica, then increases taking a maximum around the 15 %wt of silica and decreases afterwards. Both the dispersive and polar components follow similar tendencies with the increase in the amount of silica.

Fig. 1 displays the heat flow during the second heating scan of the DSC measurements, referred to each sample mass (specific heat power). Curves of the specific heat capacity (up to a constant) against temperature were calculated by dividing the curves in Fig. 1 through the heating rate, and employed to determine the glass transition temperature, T_g, for each composition as the inflexion point of these curves. The width of the glass transition, ΔT_g, was determined as the temperature interval defined by the intersections of the tangent line at the inflexion point and the extrapolated glass and liquid lines. The specific heat capacity increment at the glass transition measured per gram of hybrid, Δc_p, has been obtained as the difference between these intersections at T_g. The mass fraction of hybrid material able to undergo conformational motions at the glass transition, *x*, and the mass fraction of copolymer in the hybrid able to undergo conformational motions at the glass transition, *x*′, have been calculated as [20,21]:

$$x = \frac{\Delta c_p}{\Delta c_p^{\text{copolymer}}} \qquad x' = \frac{\Delta c_p}{\Delta c_p^{\text{copolymer}}\cdot x_{\text{copolymer}}} = \frac{x}{x_{\text{copolymer}}} \tag{4}$$

where $x_{\text{copolymer}}$ is the mass fraction of copolymer in the hybrid. These four parameters have been represented in Fig. 2.

Both PEMA and PHEA are amorphous polymers with glass transition temperatures of 81.87 and 11.37 °C, respectively. The single glass transition of the copolymer lies between those of the homopolymers, shifts to higher

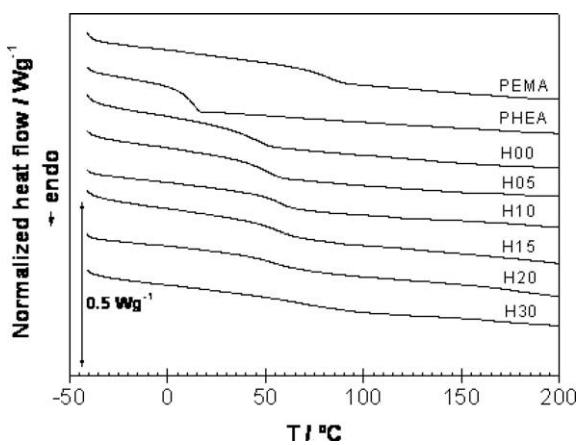

Fig. 1. Normalized heat flow during the second calorimetric heating scan.

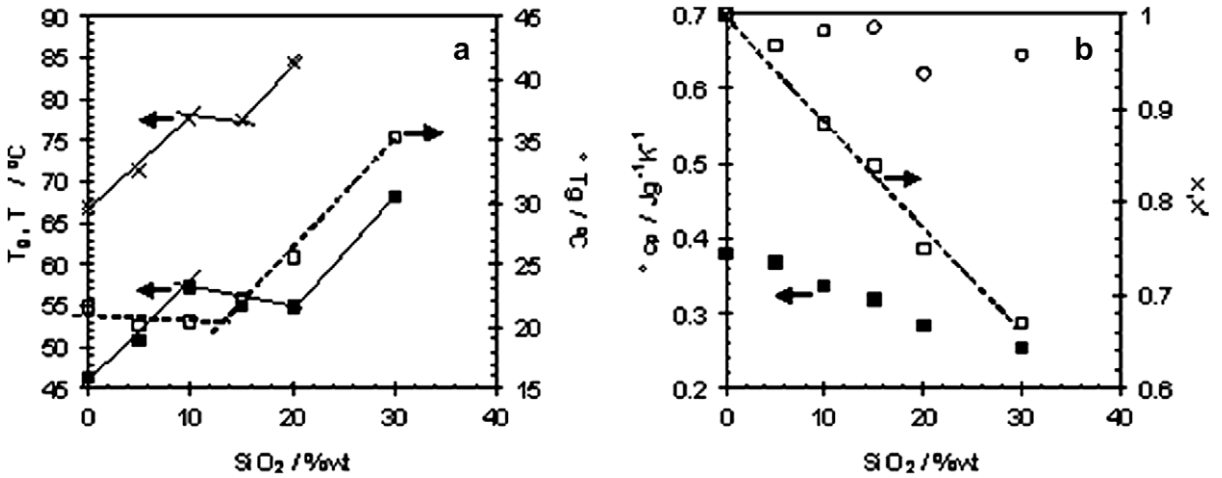

Fig. 2. (a): (■) DSC glass transition temperature (T_g), (×) temperature of the maximum loss tangent (T_α), and (□) width of the glass transition (ΔT_g); (b): (■) specific heat capacity jump (Δc_p) at the glass transition and (□) fraction of the hybrid able to undergo the glass transition process (x) and (○) fraction of the copolymer able to undergo the glass transition process (x') as a function of the silica content.

temperatures, and broadens tending to vanish with the increase of the silica content, being hardly discernible for the H30 hybrid. The T_g of the copolymer, 46.33 °C, increases 10 °C when adding a 10 %wt of silica, then remains stable up to 20 %wt, and increases 10 °C more for the 30 %wt of silica. The ΔT_g is 20.74 °C for PEMA, 9.87 °C for PHEA and 21.75 °C for the copolymer. For the hybrids it takes values similar to the copolymer up to 10 %wt of silica, when it starts to increase as the glass transition broadens. The Δc_p for PEMA is 0.31 J/gK, for PHEA it is 0.44 J/gK and for the copolymer it is 0.38 J/gK. It decreases linearly with the silica content. The fraction of the hybrids undergoing conformational motions at the glass transition, x, decreases linearly from unity for the copolymer to 0.67 for H30, but the fraction of copolymer in the hybrids able to participate in the glass transition, x', is always close to unity.

Fig. 3 shows the dynamic-mechanical spectra obtained for both homopolymers and the copolymer, in the temperature range from −60 to 200 °C, in terms of the storage modulus, E', and loss tangent, tan δ.

The PHEA homopolymer presents the single peak in tan δ in this interval of temperatures, with the maximum at 35.6 °C, characterizing its main relaxation process associated to the glass transition, whereas PEMA presents it at 101.4 °C. The possible secondary relaxations lie below the analysed temperature interval. The main relaxation process corresponding to the copolymer lies between the ones corresponding to both homopolymers. It appears as a sharp single drop of the storage modulus, with the corresponding maximum of the loss tangent at 67.20 °C.

The curves corresponding to the nanocomposites were obtained in the temperature range of 25–200 °C, since no

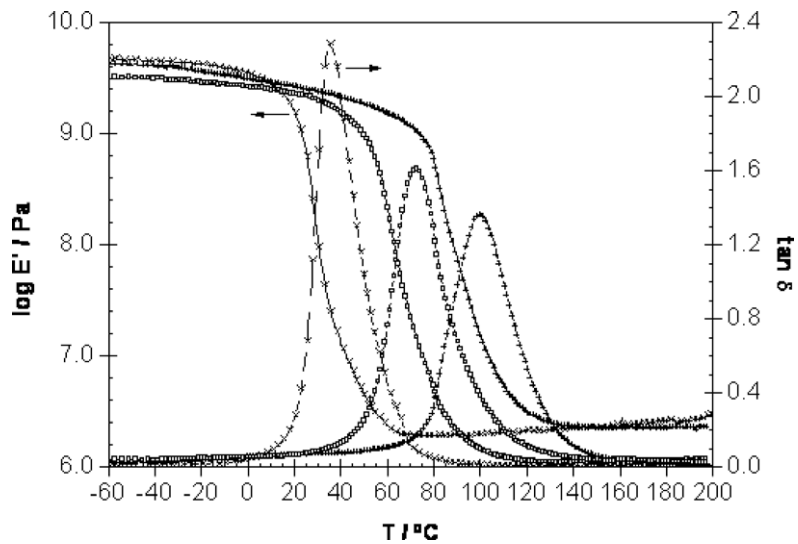

Fig. 3. Temperature dependence of (—) the storage modulus (E') and (- -) loss tangent (tan δ) of: (+) PEMA, (×) PHEA and (□) H00.

relaxation was expected to take place at lower temperatures, and are displayed in Fig. 4. The measurements with the H30 samples could not be performed because they broke when being clamped. The main relaxation progressively shifts to higher temperatures and broadens, becoming more asymmetric when the silica content increases. In addition, the rubbery plateau modulus increases. The temperatures of the maxima in tan δ, T_α, and the storage moduli of the samples at 150 °C, $E'_{150\,^\circ C}$, have been represented in Figs. 2 and 5(a). The T_α increases linearly with the increase of the silica content. The $E'_{150\,^\circ C}$ values for PEMA, PHEA and H00 are 2.30, 2.27 and 1.10 MPa, respectively. The plateau modulus does not vary significantly up to 10 %wt of silica, when it starts to increase steeply, following an exponential tendency.

At temperatures above 150 °C the storage moduli of the H10, H15 and H20 hybrids increase approximately 1.5-fold. This effect has been reported in the literature [22,23] and attributed to molecular motions at high temperatures allowing uncompleted sol–gel reactions to continue. In order to confirm this hypothesis, the H15 specimen was allowed to cool to 120 °C and rescanned again. The thermogram obtained is inserted in Fig. 4(a) and shows that the change operated in the sample during the first scan is irreversible, and the modulus maintains its value when cooling and increases but to a lesser extent when rescanning.

The compressive elastic moduli, E, have been obtained from the stress–strain curves, and are shown in Fig. 5(b). The values obtained for the homopolymers are 4193 and 142 MPa for PEMA and PHEA, respectively. The elastic modulus of the copolymer lies between those of the homopolymers, and maintains similar values up to H15, from where it starts to increase. The elastic modulus of H30 is similar to that of PEMA.

4. Discussion

Hybrid nanocomposites of P(EMA-*co*-HEA) 70/30 %wt – SiO_2 can be successfully obtained with the procedure here

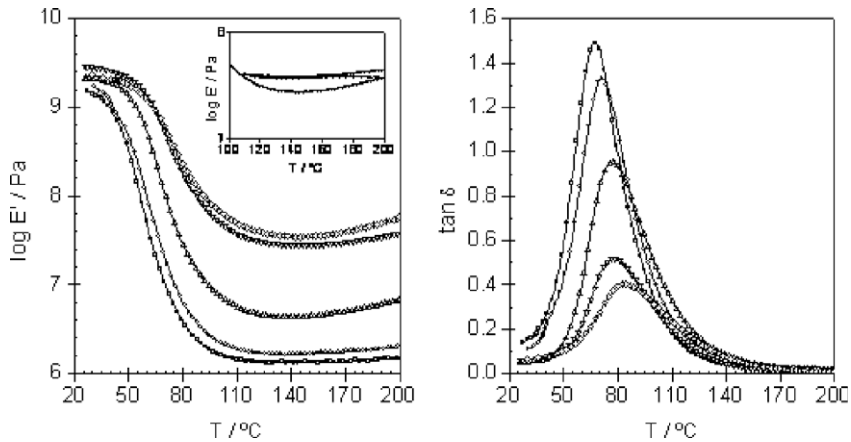

Fig. 4. Temperature dependence of (—) the storage modulus (E') and (- -) loss tangent (tan δ) for P(EMA-*co*-HEA)/SiO_2 nanohybrids, with: (□) 0, (○) 5, (△) 10, (▽) 15 and (◇) 20 %wt SiO_2. Inset: evolution of E' with a cycling temperature program of a first heating until 200 °C, an immediate cooling until 110 °C and a reheating, for H15.

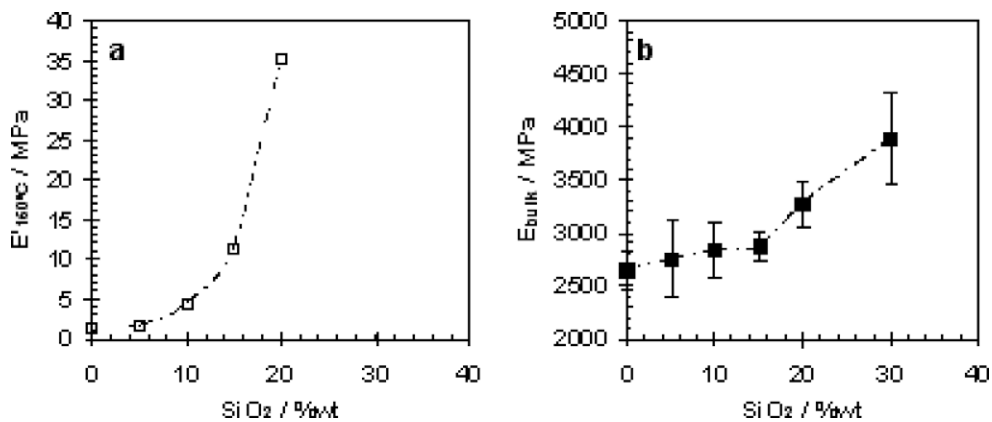

Fig. 5. Dependence of (a) the storage modulus at 150 °C ($E'_{150\,^\circ C}$) obtained from DMS measurements and (b) elastic modulus (E) obtained from compression tests, with the silica content.

described. Notwithstanding the poor miscibility of the silica precursor and the EMA monomer, the presence of the HEA comonomer compatibilizes the mixture and the resulting materials are homogeneous, giving rise to samples which were optically transparent and increasingly rigid as the percentage of silica increased. However, the condensation reactions are still possible after the sample preparation procedure: the dynamic-mechanical results show that at temperatures above 150 °C, molecular motions allow sol–gel reactions to start again, leading to a higher connectivity of the silica network. This effect explains the slight increase in the storage modulus at these temperatures, and has been observed by other authors [22,23]. Water produced in these condensations could be involved in the accelerated chain scissions of the organic copolymer in the thermogravimetric assays [15]. At temperatures below the glass transition, the vitrified polymeric phase hinders further sol–gel reactions.

As explained in a previous work [15], these nanohybrids consist in two phases, organic and inorganic, both of them in the form of networks, finely interpenetrated. For silica contents up to 10 %wt of silica, Fig. 6, the inorganic phase is uniformly dispersed as tunneled, nanoporous nanoparticles, which join forming larger aggregates leaving spaces of tens of nanometers. Higher silica contents produce silica networks which percolate and eventually extend continuously throughout the sample, totally interpenetrated with the organic network. Only the nanohybrids with silica contents above 10 %wt left one-piece continuous residues after the thermogravimetric measurements (data not shown). The elementary nanotunneled silica units possess non-condensed silanol, Si–OH, groups all along their boundary surfaces. These silanols disappear as the percolation and the development process of the continuous silica structure proceed: the larger the amount of silica after percolation, the less the specific area of its phase boundary, and thus also the specific (with respect to silica mass) number of free silanol groups.

The contact angle results are in agreement with this picture. The low percentage of silica explains the average water contact angle of the H05 surface being approximately equal to that of the copolymer. An increase in wettability is observed on the surfaces as a consequence of the increase of the silica content and thus of the increase in the number of silanol terminal groups at the surfaces. In spite of its higher silica content, this tendency is broken by the H30 sample, which has a contact angle again similar to that of the copolymer surface. The extreme rigidity of this sample and its rough surface, however, made this datum unreliable.

The surface tension of PEMA and its dispersive and polar components here obtained agree well with those found in the literature [24], and with those obtained by Olmedilla et al. [25] in previously swollen PEMA, a result to be expected given the low water sorption of PEMA. The high water content angle on dry PHEA is due to the fact that hydroxyls are not exposed at the surface when the sample is dry. The dispersive forces and polar interactions of swollen PHEA are twice those found herein for dry PHEA, owing to its hydrophilic character [25]. The polarity of the copolymer is, strangely, slightly lower than that of PEMA, and increases with the silica content up to a value close to PHEA for H20, due to the increasingly hydrophilic character of the surfaces of the hybrids. This confirms that the influence of silica is felt also on the samples' surfaces. This is of great importance since the hydrophilic character of the surfaces plays an important role during apatite formation [6,26–28]. The presence of Si–OH groups on the surface (and/or their formation by dissolution of the silica network) is related to the ability of the surface to nucleate hydroxyapatite crystals in contact with body fluids, which are supersaturated in calcium phosphate. As stated above, the steep decrease in polarity of H30 could be explained on the basis of a perfect co-continuous silica network interpenetrated with the polymeric matrix, with an insignificant amount of hydroxyl groups available at the surfaces, though the influence of other parameters such as the stiffness or the roughness of the surface cannot be excluded.

The elastic moduli of the nanocomposites measured in compression (Fig. 5(b)) and in tension at room tempera-

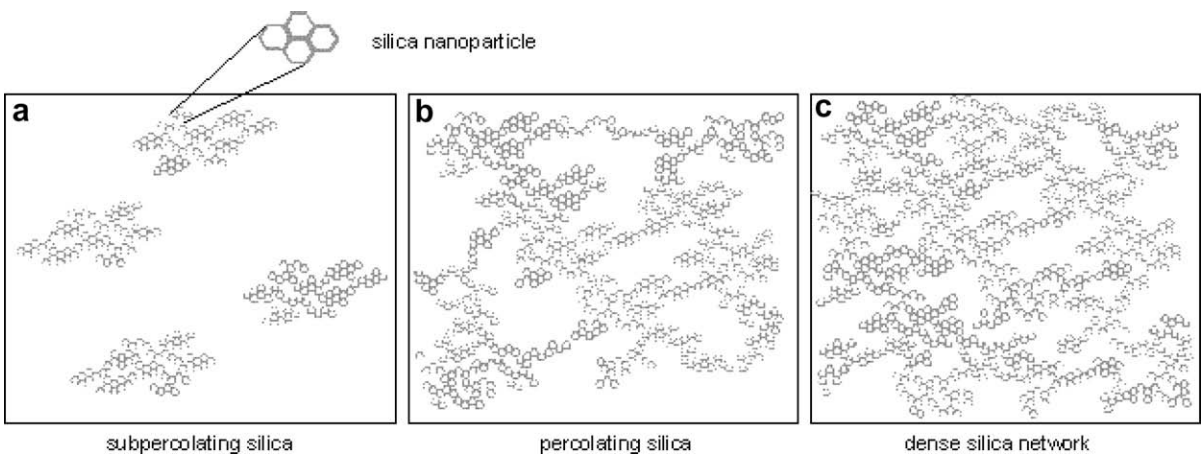

Fig. 6. Sketches of different silica network structures, according to the percentage in weight of silica, ϕ: (a) low concentration sub-percolating silica, $\phi < 15\%$ SiO_2, (b) higher concentration, about to percolate silica, $\phi \approx 15\%$ SiO_2, and (c) high concentration super-percolating silica, $\phi > 15\%$ SiO_2.

tures in the glassy state (Fig. 4(a)) show a marked change in their increasing pattern from 15 %wt of silica on, the compressive moduli being always slightly higher than the tensile moduli. The elastic modulus measured in tension in the rubbery state (Fig. 5(a)) follows the same tendency.

The calorimetric thermogram of the copolymer, with a single glass transition lying between those of the homopolymers, suggests the homogeneous nature of the copolymer at scales of sensibility of the calorimeter. The dynamic-mechanical spectra of the copolymer shows the single main relaxation process associated to the glass transition as a sharp single drop of the storage modulus with the corresponding maximum of the loss tangent, located between the curves corresponding to both homopolymers. The dynamic-mechanical relaxation process associated to the glass transition is more sensitive to phase heterogeneity than the glass transition measured by calorimetry [29], and thus the dynamic-mechanical data confirm the homogeneity of the copolymer and the inexistence of phase separation. Though related, T_g and T_α (obtained from DSC and DMS measurements, respectively) reflect differently the main relaxation process of the polymer: besides the just mentioned differing sensitivity of both, one must also bear in mind that T_α is frequency dependent. Thus, it is natural that T_g and T_α have not exactly coincident tendencies. Nonetheless, our results show a close match of the increment of both temperatures, around 20 °C, as the silica content increases from 0 to 20 %wt (see Fig. 2(a)). The general increase in T_g and the gradual shift to high temperatures of its associated mechanical relaxation with increasing silica contents has been observed previously by other authors [23,30], and points to the restriction of polymer chain mobility as they become more intertwined with the rigid silica network, resulting in a mechanical reinforcing effect. The compressive elastic moduli of the nanocomposites increase from 15 to 30 %wt of silica, up to a value for H30 close to that of PEMA, owing to this silica reinforcing effect. The elastic moduli of the nanohybrids are expected to increase even more in contact with biological fluids, due to hydroxyapatite coating, up to values closer to that of the elastic human dentin modulus, 14.47 GPa [31].

Since these systems do consist in two networks interpenetrated at a molecular level, the question arises whether the close presence of the inorganic network might affect the relaxation behaviour of the organic network. At first sight, the decrease in Δc_p seems to suggest that, as the amount of silica in the sample increases, the number of polymer chains able to participate in the glass transition process decreases. However, the fraction of copolymer able to undergo conformational motions at the glass transition is always close to unity, which indicates that almost all the copolymer chains existent in the hybrids are able to participate in the glass transition process, and thus no complete confinement or total restriction effect can be ascertained. Nonetheless, the silica network hinders to some degree the polymer chain motions, as it broadens the glass transition process. In parallel, the main mechanical relaxation broadens, decreases in intensity and shifts to higher temperatures. The progressive disappearance of the calorimetric glass transition with the increase in silica content has already been observed by other authors [22,32]. They attributed the absence of a clear calorimetric glass transition to the confinement of the polymer chains in domains smaller than 15 nm, of the order of size of the cooperatively rearranging region. Despite the important drop of the heat capacity increment at the glass transition in the samples over a 20 %wt of silica the relaxation process has not disappeared completely, since it is still detected by the dynamic-mechanical measurements through its associated main relaxation, and confirmed by the high value of x' in Fig. 2(b).

The build-up of structure with increasing silica content is reflected in the composites' properties. The percolation of the dispersed silica nanophase and its development into a continuous network can be followed in the kinked-shaped curves of ΔT_g and of E (Figs. 2 and 5). Consistently with these observations, only for super-percolating silica contents were integral residues obtained after performing a pyrolysis removing the organic phase [15]. Some authors [33] have attributed the increase of the rubbery plateau modulus to the polymer chains extending into the nanoscale silica network with relatively strong hybrid hydrogen bondings. In our case, this type of explanation would be difficult to reconcile with the impoverished thermal stability of the hybrids discussed elsewhere [15].

5. Conclusions

Homogeneous hybrid nanocomposite materials of P(EMA-*co*-HEA) 70/30 %wt / SiO_2 with varying proportions of silica up to 30 %wt can be obtained by the simultaneous sol–gel polymerization of the inorganic and the organic networks. Different phase morphologies of the silica network within the copolymeric matrix are obtained as a function of silica contents, and these differences affect the physico-chemical properties of the surfaces (wettability, surface tension). The surface tension and polarity of the surfaces increase with silica contents between 5 and 20 %wt, owing to the increase in the number of silanol terminal groups at the surfaces. However, higher silica contents render less terminal non-condensed silanol groups accessible when a denser continuous silica interpenetrated network has formed, and the materials' surface energies fall again to values similar to that of the copolymer. The build-up of the silica phase connectivity, from sub-percolating proportions to an extended dense network, is reflected in characteristic inflections around the percolation threshold of properties such as the rubbery modulus and the glass transition width.

The effect of the constraining silica phase on the relaxation behaviour of the organic polymer is patent, though a complete immobilization of polymer chains due to that constraint cannot be ascertained. It translates into an increase of the glass transition temperature and, more pronounced, a shift of its associated mechanical relaxation to higher temperatures, which can be attributed to the restriction of the motion of the copolymer chains as they are more intertwined with the rigid silica network. The glass transition process smoothens and the main dynamic-mechanical relaxation broadens, but practically all the copolymer chains in the nanocomposites are able to undergo conformational motions at the glass transition.

An important mechanical reinforcing effect can be achieved with this type of silica filling of polymer matrices, as reflected in the compressive elastic moduli and the rubber moduli of the nanocomposites.

The interplay of network connectivity and free silanol groups in these kind of nanocomposites leads to remarkable properties from the point of view of the intended applications of these materials: nanohybrids with intermediate silica contents (10–20 %wt) exhibit an interesting balance between (i) mechanical reinforcement attained by a nearly developed co-continuous silica networks and (ii) enhanced surface reactivity or hydrophilicity due to the still elevated specific content of polar silanol terminal groups.

Acknowledgements

G.G.F. and M.M.P. acknowledge the support by funds for research in the field of Regenerative Medicine through the collaboration agreement from the Conselleria de Sanidad (Generalitat Valenciana), and the Instituto de Salud Carlos III (Ministry of Science and Innovation). This paper is part of the work titled "P(EMA-*co*-HEA)/SiO_2 nanohybrid scaffolds for guided dentin regeneration" awarded with the prize for Research in Odontostomatology of the Vitaldent Foundation in its VI International Edition (2009).

References

[1] Hench LL, Splinter RJ, Allen WC, Greenlee TK. Bonding mechanisms at the interface of ceramic prosthetic materials. J Biomed Mater Res Symp 1972;2:117–41.
[2] Li R, Clark AE, Hench LL. An investigation of bioactive glass powders by sol-gel processing. J Appl Biomat 1991;2:231–9.
[3] Kokubo T. Bioactive glass ceramics: properties and applications. Biomaterials 1991;12:155–63.
[4] Ohtsuki C, Kokubo T, Yamamuro T. Mechanism of apatite formation on CaO–SiO_2–P_2O_5 glasses in a simulated body fluid. J Non-Cryst Solids 1992;143:84–92.
[5] Zhong J, Greenspan DC. Processing and properties of sol–gel bioactive glasses. J Biomed Mater Res Appl Biomater 2000;53:694–701.
[6] Salinas AJ, Vallet-Regi M, Izquierdo-Barba I. Biomimetic apatite deposition on calcium silicate gel glasses. J Sol–Gel Sci Tech 2001;21:13–25.
[7] Cerruti M, Morterra C. Carbonate formation on bioactive glasses. Langmuir 2004;20:6382–8.
[8] Du R, Chang J. Preparation and characterization of bioactive sol–gel derived $Na_2Ca_2Si_3O_9$. J Mater Sci Mater Med 2004;15:1285–9.
[9] Kokubo T. Design of bioactive bone substitutes based on biomineralization process. Mater Sci Eng C 2005;25:97–104.
[10] Huang W, Day DD, Kittiratanapiboon K, Rahaman MN. Kinetics and mechanisms of the conversion of silicate (45S5), borate, and borosilicate glasses to hydroxyapatite in dilute phosphate solutions. J Mater Sci Mater Med 2006;17:583–96.
[11] Hench LL. The story of Bioglass®. J Mater Sci Mater Med 2006;17:967–78.
[12] Ben-Nissan B, Ylänen HO. Bioactive glasses and glass ceramics. In: Akay M, editor. Wiley enciclopedia of biomedical engineering. New Jersey: John Wiley & Sons; 2006. p. 354–66.
[13] Kokubo T, Takadama H. How useful is SBF in predicting in vivo bone bioactivity? Biomaterials 2006;27:2907–15.
[14] Kim HM, Himeno T, Kokubo T, Nakamura T. Process and kinetics of bonelike apatite formation on sintered hydroxyapatite in a simulated body fluid. Biomaterials 2005;26:4366–73.
[15] Vallés-Lluch A, Rodríguez-Hernández JC, Gallego Ferrer G, Monleón Pradas M. Synthesis and characterization of P(EMA-*co*-HEA)/SiO_2 nanohybrids for mineralized tissue regeneration. Eur Polym J, submitted for publication [EUROPOL D 0901511].
[16] Neumann AW, Spelt JK, editors. Applied surface thermodynamics. surfactant science series, vol. 63. New York: Marcel Dekker; 1993.
[17] Owens DK, Wendt RC. Estimation of surface free energy of polymers. J Appl Polym Sci 1969;13:1741.
[18] Busscher HJ, Vanpelt AWJ, Deboer P, Dejong HP, Arends J. The effect of surface roughening of polymers on measured contact angles of liquids. Colloids Surf 1984;9:319–31.
[19] Birdi KS. Surface tension of polymers. In: Yildrim Erbil H, editor. CRC Handbook of surface and colloid chemistry. Boca Raton: CRC Press; 1997. p. 292.
[20] Privalko VP, Lipatov YS, Kercha YY. Calorimetric study of the phase boundary effect on oligo-ethylene glycol adipate (OEGA) properties. Polym Sci USSR 1970;12:1520–9.
[21] Lipatov YS, Privalko VP. Glass transition in filled polymer systems. Polym Sci USSR 1972;14:1843–8.
[22] Hajji P, David L, Gerard JF, Pascault JP, Vigier G. Synthesis, structure and morphology of polymer-silica hybrid nanocomposites based on hydroxyethyl methacrylate. J Polym Sci Part B Polym Phys 1999;37:3172–87.
[23] Rodríguez Hernández JC, Monleón Pradas M, Gómez Ribelles JL. Properties of poly(2-hydroxyethyl acrylate)-silica nanocomposites obtained by the sol–gel process. J Non-Cryst Solids 2008;354:1900–8.
[24] Van Krevelen DW, editor. Properties of polymers. New York: Elsevier; 1997. p. 238.
[25] Olmedilla MP, García-Giralt N, Pradas MM, Ruiz PB, Ribelles JLG, Palou EC, et al. Response of human chondrocytes to a non-uniform distribution of hydrophilic domains on poly(ethyl acrylate-co-hydroxyethyl methacrylate) copolymers. Biomaterials 2006;27(7):1012–33.
[26] Oliveira AL, Malafaya PB, Reis RL. Sodium silicate gel as a precursor for the in vitro nucleation and growth of a bone-like apatite coating in compact and porous polymeric structures. Biomaterials 2003;24:2575–84.
[27] Oyane A, Uchida M, Choong C, Triffitt J, Jones J, Ito A. Simple surface modification of poly(ε-caprolactone) for apatite deposition from simulated body fluid. Biomaterials 2005;26:2407–13.
[28] Rhee SH. Effect of molecular weight of poly(e-caprolactone) on interpenetrating network structure, apatite-forming ability, and degradability of poly(ε-caprolactone)/silica nano-hybrid materials. Biomaterials 2003;24:1721–7.
[29] Ward IM, Hadley DW. An introduction to the mechanical properties of solid polymers. England: Wiley; 1993.
[30] Costa ROR, Vasconcelos WL. Structural modification of poly(2-hydroxyethyl methacrylate)-silica hybrids utilizing 3-methacryloxypropyltrimethoxysilane. J Non-Cryst Solids 2002;304:84–91.
[31] Craig RG, Peyton FA. Elastic and mechanical properties of human dentin. J Dent Res 1958;37(4):710–8.
[32] Motomatsu M, Takahashi T, Nie HY, Mizutani W, Tokumoto H. Microstructure study of acrylic polymer-silica nanocomposite surface by scanning force microscopy. Polymer 1997;38:177–82.
[33] Huang SL, Chin WK, Yang WP. Structural characteristics and properties of silica/poly(2-hydroxyethyl methacrylate) (PHEMA) nanocomposites prepared by mixing colloidal silica or tetraethyloxysilane (TEOS) with PHEMA. Polymer 2005;46:1865–77.